



Effects of water and iron content on the rheological contrast between garnet and olivine

Ikuo Katayama*, Shun-Ichiro Karato

Department of Geology and Geophysics, Yale University, New Haven, CT 06520, USA

Received 7 December 2006; received in revised form 18 October 2007; accepted 23 October 2007

Abstract

The effects of water and iron content on the relative creep strengths of garnet and olivine were investigated by shear deformation experiments. Garnet and olivine samples were sandwiched together between alumina pistons in a simple shear geometry and were deformed at $P=1\text{--}2\text{ GPa}$, $T=1473\text{ K}$ and strain rates ranging from 10^{-5} to 10^{-3} s^{-1} using a Griggs-type solid-medium apparatus. The stress- and strain-rate relation, as well as the deformation microstructures including lattice-preferred orientation and dynamic recrystallization, indicates that the deformation by dislocation creep. The creep tests show that the Fe-rich garnet ($\text{Alm}_{67}\text{Prp}_{29}\text{Grs}_3$) was slightly weaker than olivine (Fo90), whereas the Mg-rich garnet ($\text{Alm}_{19}\text{Prp}_{68}\text{Grs}_{12}$) was significantly stronger than olivine under dry conditions. The wet experiments show that the creep rate of the Mg-rich garnet is more sensitive to water than olivine; the water fugacity exponent on strain rate was estimated to be ~ 2.4 for garnet and ~ 1.2 for olivine, and the Mg-rich garnet becomes weaker than olivine in a water-rich environment. The experimental results show that the rheological contrast between garnet and olivine depends strongly on water content and to a lesser degree on Fe content. Consequently, the geodynamic behavior of geochemical reservoirs can be sensitive to their chemical environments in the upper mantle.

© 2007 Elsevier B.V. All rights reserved.

Keywords: Rheological contrast; Water; Garnet; Olivine; Geochemical reservoir; Upper mantle

1. Introduction

One of the most important on-going process of geochemical evolution in the Earth is partial melting at mid-ocean ridges. This partial melting creates relatively enriched basaltic crust and residual “depleted” peridotite. The geodynamic behavior of such geochemically distinct reservoirs is mainly controlled by their density and rheological contrast with the surrounding mantle rocks (Ringwood and Irifune, 1988; Manga, 1996; Karato, 1997). Garnet and olivine are two minerals that are representative of the two most important geochemical reservoirs of the Earth’s upper mantle (Irifune and Ringwood, 1987). Garnet is the major mineral in the silica-rich, less depleted component (e.g., subducted oceanic crust), whereas olivine is the major mineral in the depleted component. Consequently, the contrast in physical properties between garnet and olivine have

an important influence on the geodynamic behavior of geochemical reservoirs in the upper mantle. Although the density contrasts between these two components have been systematically investigated (e.g., Ringwood and Irifune, 1988), little is known about the rheological contrast, particularly the rheological behavior of garnet. Previous study by Karato et al. (1995) focused on the systematics between the melting temperature and the creep strength of silicate garnets as well as analogue materials. Although the study of the broad systematics provided a first clue to estimate the rheological properties of garnet in the Earth’s mantle, the potentially important roles of water and of iron content have not been investigated. Since the variation of both water content and iron content in garnet can have large effects on the rheological properties, it is essential to investigate the influence of these factors. We have therefore conducted an experimental study to investigate the influence of water and iron content on the rheological contrast between garnet and olivine. Our experimental results provide a clue to assess the effects of the chemical environment on the geodynamic behavior of geochemically distinct reservoirs in the upper mantle.

* Corresponding author. Present address: Department of Earth and Planetary Systems Science, Hiroshima University, Hiroshima 739-8526, Japan. Tel.: +81 824 24 7468; fax: +81 824 24 0735.

E-mail address: katayama@hiroshima-u.ac.jp (I. Katayama).

Table 1
Chemical composition of garnet

	Fe-rich	Mg-rich
wt% oxides		
SiO ₂	38.3	41.8
TiO ₂	0.0	1.3
Al ₂ O ₃	21.1	20.5
FeO ^a	30.7	10.0
MnO	0.6	0.3
MgO	7.5	19.5
CaO	0.9	4.8
Na ₂ O	0.0	0.1
K ₂ O	0.0	0.0
Total	99.1	98.3
Cations per 12 oxygen		
Si	3.02	3.05
Ti	0.00	0.07
Al	1.96	1.76
Fe	2.03	0.61
Mn	0.04	0.02
Mg	0.88	2.12
Ca	0.07	0.37
Na	0.00	0.01
K	0.00	0.00
Xprp	0.29	0.68
Xalm	0.67	0.19
Xgrs	0.03	0.12
Xsps	0.01	0.01

^a Total Fe calculated as FeO.

2. Experimental procedure

2.1. Starting materials

The starting materials were prepared from a sample of San Carlos olivine (Fo90) and two natural garnets of different chemical compositions. One garnet was Fe-rich ($\text{Alm}_{67}\text{Prp}_{29}\text{Grs}_3$) and the other Mg-rich ($\text{Alm}_{19}\text{Prp}_{68}\text{Grs}_{12}$), and the chemical compositions are shown in Table 1. Inclusion-free crystals of olivine and garnets were carefully selected and crushed using an agate mortar. The dried fine-grained powders were placed into a Ni capsule and were annealed at $P=1.0\text{--}1.5\text{ GPa}$ and $T=1573\text{ K}$ for $\sim 5\text{ h}$. The hot-pressed samples show equilibrium grain-boundaries and average grain sizes are $15\text{--}20\text{ }\mu\text{m}$ that was measured by the intercept method (Fig. 1). We measured the crystal orientation of the hot-pressed samples using electron back-scattered diffraction (EBSD). The samples show nearly random orientation and the distribution of misorientation angles follows the theoretical curve of a random distribution (Fig. 2). Water contents of the hot-pressed samples are $<\sim 200\text{ ppm H/Si}$ for olivine and $<\sim 500\text{ ppm H/Si}$ for garnets (detailed discussion to follow).

2.2. Deformation experiments

Shear deformation experiments were conducted using a Griggs-type solid-medium apparatus at $P=1\text{--}2\text{ GPa}$, $T=1473\text{ K}$, and strain rates ranging from $\sim 10^{-5}$ to $\sim 10^{-3}\text{ s}^{-1}$

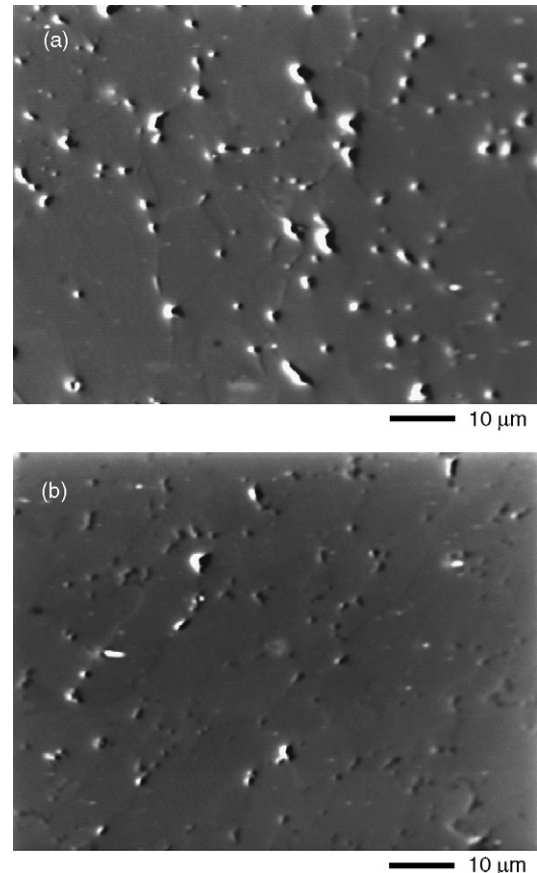


Fig. 1. Secondary electron images of the hot-pressed starting materials (a) olivine and (b) garnet.

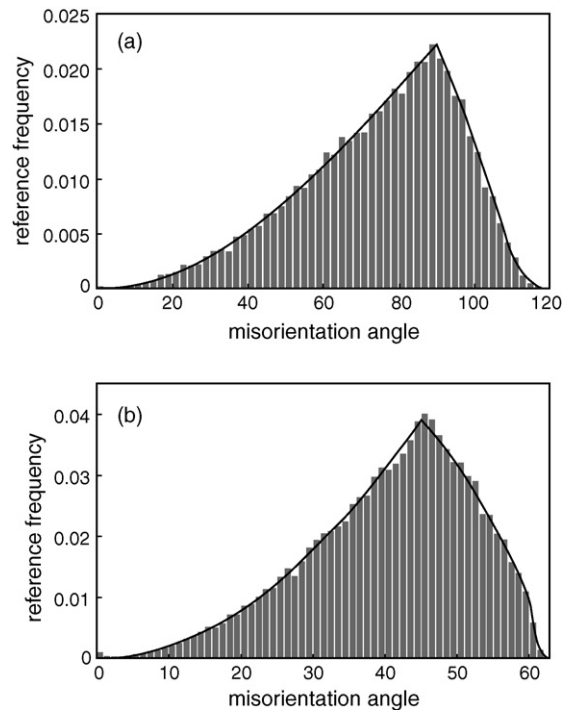


Fig. 2. Misorientation angle distributions of the starting material (a) olivine and (b) garnet, which follow the theoretical curve (thick line) for a random orientation.

Table 2
Experimental conditions and results

Sample	Phase	Composition	Pressure (GPa)	Temperature (K)	Compressional strain (%)	Shear strain (γ) ^a	Strain rate (s^{-1})	Dislocation density ($\times 10^{12} m^{-2}$) ^b	Stress (MPa) ^c	Water content (H/ $10^6 Si$) ^d
GA-069	Garnet	Alm-rich dry	1.0	1473	12	1.0 (± 0.1)	$1.2 (\pm 0.1) \times 10^{-4}$	3.42 (± 0.60)	290 (± 40)	520 (± 240)
	Olivine	Fo90	1.0	1473	16	0.6 (± 0.02)	$7.7 (\pm 0.3) \times 10^{-5}$			180 (± 50)
GA-079	Garnet	Alm-rich dry	1.0	1473	8	1.4 (± 0.1)	$7.9 (\pm 0.3) \times 10^{-4}$	6.89 (± 1.18)	490 (± 70)	n.a.
	Olivine	Fo90	1.0	1473	10	1.3 (± 0.1)	$7.6 (\pm 0.3) \times 10^{-4}$			<130
GA-095	Garnet	Alm-rich dry	1.0	1473	20	1.1 (± 0.1)	$5.0 (\pm 0.5) \times 10^{-5}$	2.85 (± 0.60)	240 (± 40)	230 (± 90)
	Olivine	Fo90	1.0	1473	12	0.9 (± 0.1)	$4.2 (\pm 0.5) \times 10^{-5}$			210 (± 30)
GA-108	Garnet	Alm-rich dry	1.0	1473	14	2.4 (± 0.1)	$1.3 (\pm 0.1) \times 10^{-4}$	3.52 (± 0.73)	310 (± 50)	400 (± 80)
	Olivine	Fo90	1.0	1473	13	1.5 (± 0.2)	$8.3 (\pm 1.2) \times 10^{-5}$			<140
GA-100	Garnet	Alm-rich dry	2.0	1473	15	2.0 (± 0.2)	$1.4 (\pm 0.2) \times 10^{-4}$	3.81 (± 0.78)	350 (± 60)	510 (± 100)
	Olivine	Fo90	2.0	1473	26	1.7 (± 0.4)	$1.2 (\pm 0.3) \times 10^{-4}$			200 (± 90)
GA-110	Garnet	Alm-rich dry	2.0	1473	19	1.5 (± 0.2)	$7.3 (\pm 1.0) \times 10^{-5}$	3.31 (± 0.57)	290 (± 40)	450 (± 90)
	Olivine	Fo90	2.0	1473	13	1.2 (± 0.1)	$5.8 (\pm 0.4) \times 10^{-5}$			<140
GA-128	Garnet	Alm-rich dry	2.0	1473	18	2.4 (± 0.2)	$4.2 (\pm 0.5) \times 10^{-4}$	7.36 (± 0.82)	520 (± 70)	<100
	Olivine	Fo90	2.0	1473	18	2.1 (± 0.3)	$3.9 (\pm 0.4) \times 10^{-4}$			170 (± 30)
GA-103	Garnet	Prp-rich dry	2.0	1473	9	0.4 (± 0.1)	$1.8 (\pm 0.2) \times 10^{-5}$	3.51 (± 0.93)	320 (± 60)	480 (± 100)
	Olivine	Fo90	2.0	1473	16	2.2 (± 0.2)	$9.3 (\pm 1.0) \times 10^{-5}$			190 (± 20)
GA-104	Garnet	Prp-rich dry	2.0	1473	10	0.4 (± 0.1)	$4.2 (\pm 0.4) \times 10^{-5}$	4.73 (± 0.96)	390 (± 70)	560 (± 80)
	Olivine	Fo90	2.0	1473	20	1.9 (± 0.2)	$1.9 (\pm 0.3) \times 10^{-4}$			210 (± 20)
GA-106 ^e	Garnet	Prp-rich wet	2.0	1473	18	1.0 (± 0.2)	$3.5 (\pm 0.5) \times 10^{-5}$	1.64 (± 0.27)	200 (± 30)	1250 (± 300)
	Olivine	Fo90 wet	2.0	1473	23	1.5 (± 0.2)	$5.1 (\pm 0.7) \times 10^{-5}$			450 (± 30)
GA-126 ^e	Garnet	Prp-rich wet	2.0	1473	25	2.5 (± 0.2)	$1.8 (\pm 0.2) \times 10^{-4}$	1.66 (± 0.24)	180 (± 30)	3350 (± 550)
	Olivine	Fo90 wet	2.0	1473	20	2.1 (± 0.3)	$1.6 (\pm 0.1) \times 10^{-4}$			1200 (± 170)

^a Shear strain was measured from the rotation of strain-marker. The uncertainty of the shear strain was estimated from the shape of the strain-marker.

^b Average dislocation density was estimated from ~20 olivine grains in each sample and the number in parenthesis is one standard deviation.

^c Stress was calculated from the dislocation density, and this technique has ~15% error on the stress estimate due to the calibration and heterogeneity of the dislocation density.

^d Water content was analyzed by FTIR after each experiment and calculated based on Paterson (1982) calibration for olivine and Bell et al. (1995) calibration for garnet. The uncertainty comes from several analyses of different area for each sample.

^e Talc and brucite mixture was used as a pressure medium in these wet experiments. MgO pressure medium for other experiments.

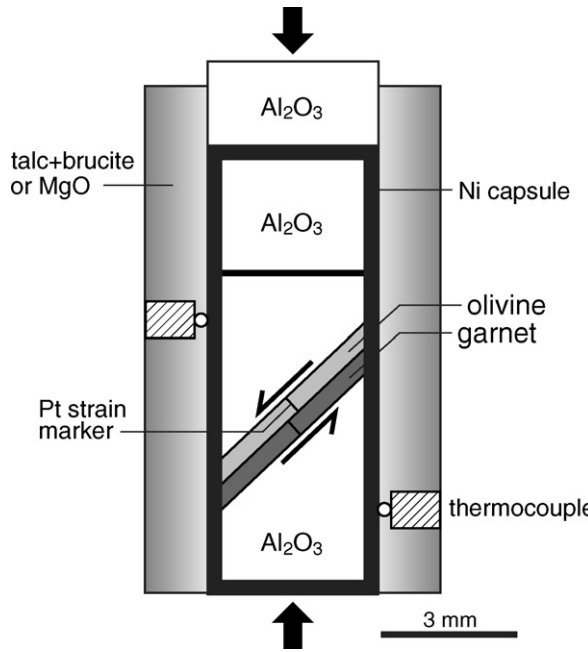


Fig. 3. Experimental configuration of the two-layer shear deformation experiments. The olivine and garnet samples were sandwiched together between the alumina pistons, which are cut at 45° from the maximum compression direction.

(Table 2). Thin slices of garnet and olivine samples (~ 0.3 mm thick each) were sandwiched together between alumina pistons in a simple shear geometry (Fig. 3). Pressure was first raised to the desired value, and then temperature was increased at a rate of ~ 30 K/min. Temperature was monitored by two Pt/Rh thermocouples placed close to the upper and lower parts of the sample (Fig. 3). The temperature variation between the two thermocouples was usually less than 20 K. After the temperature stabilized, a piston was advanced at a constant rate. Because of the large uncertainties in the stress measurements involved in a solid-medium apparatus (e.g., Green and Borch, 1989), we use the dislocation density of olivine as an indicator of the differential stress. The dislocation density piezometer was calibrated using a gas-medium apparatus (and hence the stress was well constrained), as it is known to be insensitive to water content (Karato and Jung, 2003). The dislocation density is measured in each sample after oxidation at 1173 K for 1 h. The oxidized dislocations are observed by the back-scattered electron (BSE) imaging (for details, see Karato, 1987). We measured the total length of dislocations per unit volume from the BSE images by calculating the effective thickness from which the back-scattered electrons are generated (for details see Karato and Lee, 1999). The dislocation density in our polycrystal aggregates is heterogeneous due to the various crystallographic orientations and the local stresses caused by grain interactions (Fig. 4). Therefore, we measured the dislocation density of ~ 20 grains for each sample and a statistical average of dislocation density was used to infer the stress magnitude. The variation of the dislocation density is shown in Fig. 5. The scatter in the dislocation density measurements is $\sim 15\text{--}20\%$, which will be translated into the uncertainty in the stress estimate of $\sim 10\text{--}15\%$ since the dislocation density

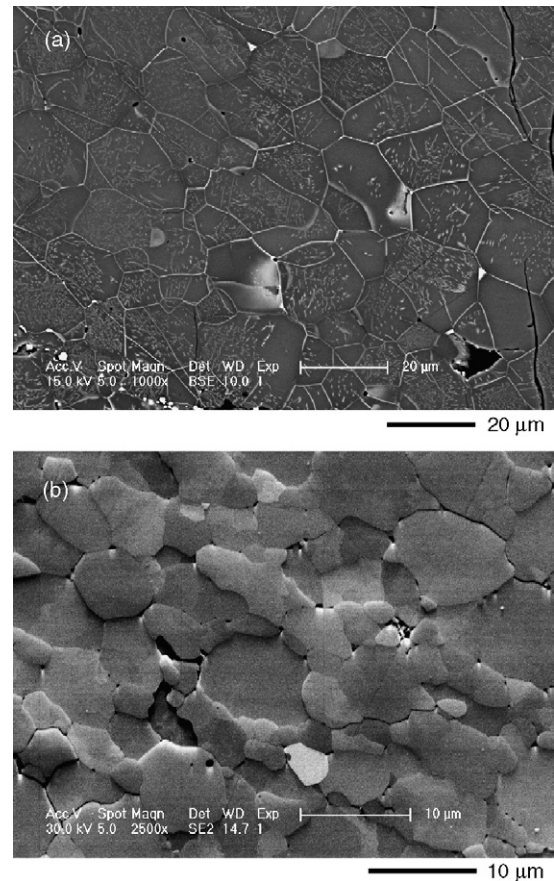


Fig. 4. (a) Back-scattered electron image of the deformed olivine sample after oxidation. Dislocations are observed as bright dots or lines within the crystals. The dislocation density is heterogeneous due to the crystallographic orientation and the local stresses, and we therefore used an average dislocation density (~ 20 grains) to infer the stress magnitude. (b) Orientation contrast image of the deformed garnet. Average grain size of the garnet is ~ 6 μm in this sample, which is significantly smaller than the starting material (~ 15 μm). The grain size reduction during the deformation is an evidence of deformation by dislocation creep. Sinistral shear in both samples.

is proportional to the power of stress (Karato and Jung, 2003). The stress level for the olivine and garnet layers should be identical in this experimental geometry. Shear strain was measured by the rotation of a platinum strain-marker, which was initially placed perpendicularly to the shear direction (Fig. 3). We also measured the compressional strain from the sample thickness before and after each experiment, and included both the shear and compressional components of strain in our analysis assuming the Levy-von Mises formulation of non-linear rheology (e.g., Karato, 2008; Chapter 3). However, the compressional effect is relatively small compared to the shear components in our experiments since the compressional strain was much smaller than the shear strain in our large strain experiments (Table 2). At the interface between the garnet and olivine layers, the chemical compositions of the samples were slightly modified during the experiments, but these regions were limited to a narrow range (<10 μm). A thin layer of NiO was observed at the interface between the Ni jacket and the samples after each experiment, suggesting that oxygen fugacity was buffered by the Ni/NiO reaction. An MgO pressure medium

was used for the dry experiments, and a mixture of talc and brucite was used as a water source for the wet experiments. In the latter case, water was supplied to the samples by the breakdown of hydrous minerals at high temperatures. For the wet experiments, the samples were kept for a few hours at the desired temperature (1473 K) before advancing the piston in order to allow hydrogen to diffuse into the sample.

2.3. Water content analysis

The water concentration in the samples was measured by Fourier-transform infrared (FTIR) spectroscopy using a mercury cadmium telluride (MCT) detector with 4 cm^{-1} resolution. The water content was calculated using the calibrations of Paterson (1982) for olivine and Bell et al. (1995) for garnet. The IR spectrum is taken from a polycrystalline specimen that contains the absorptions due to the OH-related species in the lattice as well as the grain-boundaries (Karato et al., 1986; Mei and Kohlstedt, 2000a). The IR spectra of olivine show several sharp peaks at 3360 , 3530 and 3570 cm^{-1} , and a broad peak centered at $\sim 3400\text{ cm}^{-1}$. The broad absorption band is likely to be dominated by grain-boundary water or fluid inclusions, and we have therefore subtracted this broad absorption band to calculate the intrinsic water content in the olivine (Fig. 6). The water content in the olivine is then translated into the water fugacity using the results of water solubility experiments of Kohlstedt et al. (1996) and Zhao et al. (2004). The robustness of this method has been tested in two ways. Firstly, we compared the water content in the olivine after this correction procedure was applied with the water content expected from the solubility experiments, and this showed an agreement that was better than $\sim 20\%$. Secondly, we determined the relationship between water fugacity and strain rate for the olivine, which shows a good agreement with the previous experiments. The IR spectra of garnet show a broad peak with a small shoulder at $\sim 3580\text{ cm}^{-1}$ (Fig. 6). Although the 3580 cm^{-1} peak is likely to correspond the structurally incorporated hydrogen that is due to the hydro-grossular substitution (Ackermann et al., 1983), the water content in the

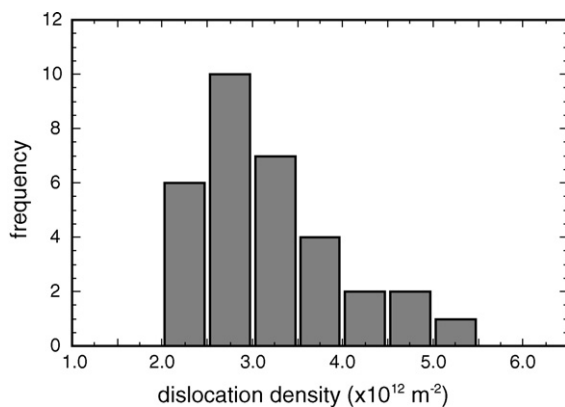


Fig. 5. A histogram of the dislocation density in the olivine (GA69). The dislocation density of each grain was measured from the back-scattered electron images of individual grains after oxidation and the histogram shows the measurement of 32 grains.

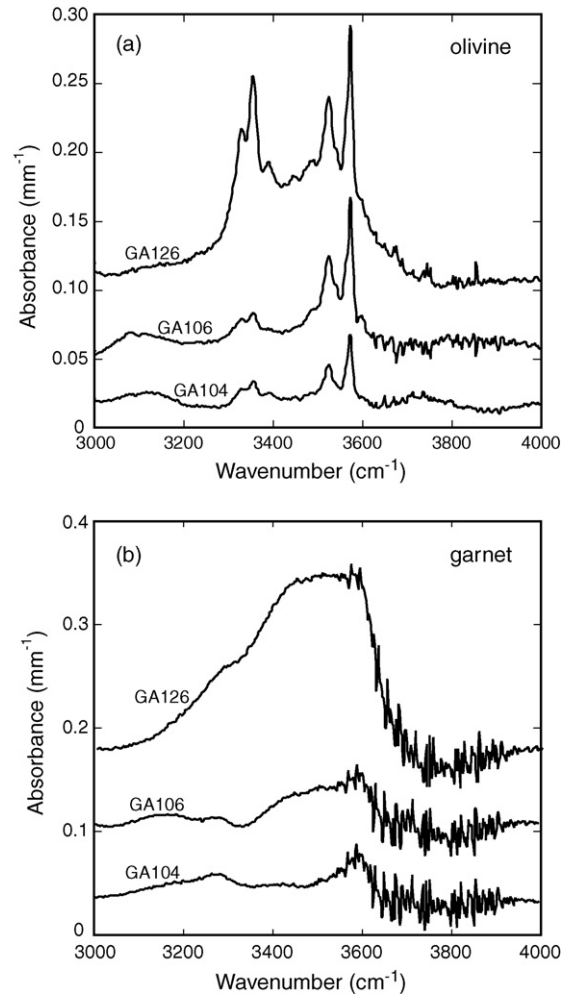


Fig. 6. Infrared spectra of olivine and garnet after experiments. (a) Olivines show sharp hydroxyl bands at 3360 , 3530 and 3570 cm^{-1} , which is related to the structurally incorporated hydroxyl. (b) Garnets show a broad band ranging 3300 – 3600 cm^{-1} with a sharp peak near 3580 cm^{-1} . The broad band is likely due to grain-boundary water or fluid inclusions, but the sharp band is related to the hydroxyl component due to the hydro-grossular substitution.

garnet has a large uncertainty because of the difficulty in defining the contribution from grain-boundary water.

3. Experimental results

The total strain rate is imposed by a given velocity of advancement of a piston, but the strain in each layer is determined only after each experiment (Fig. 7). The uncertainty in the strain rate is estimated from the shape of strain-marker, which is usually 10–20% (Table 2). Previous experiments in our laboratory showed that the steady-state deformation of olivine is achieved at a strain of ~ 0.2 (Zhang et al., 2000), and a strain of ~ 0.1 or less for garnet (Karato et al., 1995). The strain magnitude in the present study is typically ~ 1.0 . We therefore consider the relation of stress versus strain rate estimated in this way corresponds approximately to steady-state deformation. The stress value was estimated from the dislocation density, which corresponds to the stress at the latest stage of deformation. Since the stress should be identical between the two layers, the contrast in strain pro-

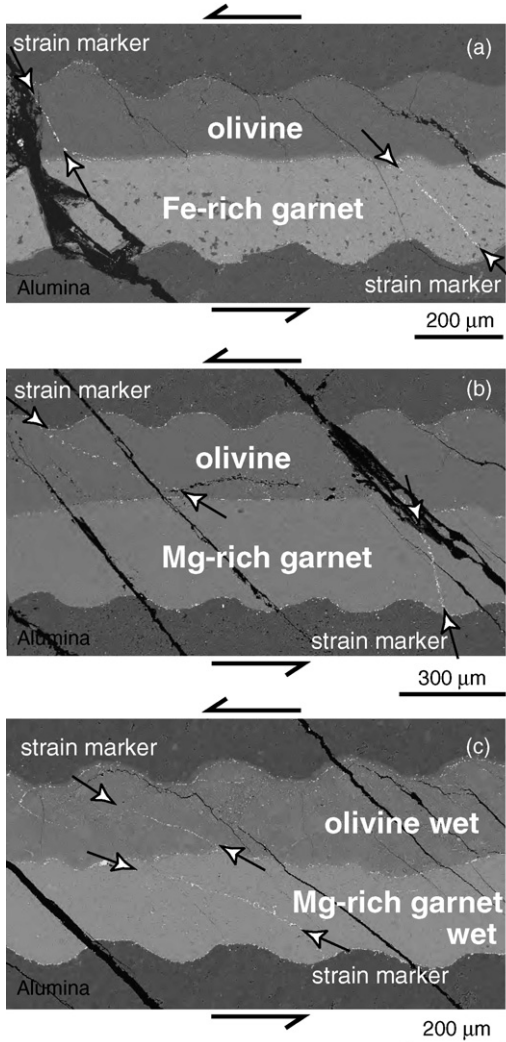


Fig. 7. Back-scattered electron images of the deformed samples. The top and bottom arrows indicate a sense of shear. The platinum strain-marker (bright line in samples) was originally perpendicular to the sample plane, and the strain was estimated from the rotation of the strain-marker in each sample, indicated by the open arrows. (a) Olivine and Fe-rich garnet at a dry condition, (b) olivine and Mg-rich garnet at a dry condition, and (c) olivine and Mg-rich garnet at a water-rich condition.

vides a good estimate of the contrast in strain rate at exactly the same stress, temperature, pressure and water fugacity.

The most commonly used flow law to analyze rheological data is the power-law formula of:

$$\dot{\varepsilon} = A\sigma^n \exp\left(-\frac{E^* + PV^*}{RT}\right) \quad (1)$$

where $\dot{\varepsilon}$ is the strain rate, A is a constant, σ is the stress, n is the stress exponent, E^* and V^* are the activation energy and volume, R is the gas constant, and P and T are the pressure and temperature (e.g., Poirier, 1985, Chapter 3). This relation indicates that the strain rate is proportional to the power of the applied stress at the given temperature and pressure. The stress exponent is known to be sensitive to the deformation mechanism, such as $n \sim 1$ for diffusion creep and $n \sim 3–5$ for dislocation creep (e.g., Poirier, 1985, Chapter 3). The mechanical data in our

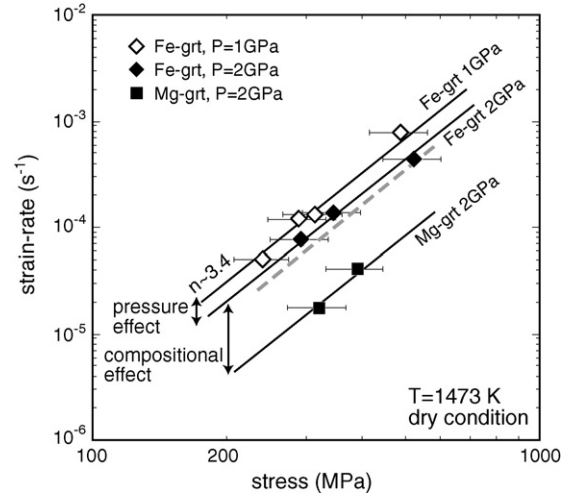


Fig. 8. Stress- and strain-rate curve of the garnets deformed at $P = 1–2$ GPa, $T = 1473$ K under dry conditions. The power-law relation between stress and strain rate gives a stress exponent $n \sim 3.4$, suggesting deformation in the dislocation creep regime. The Mg-rich garnet shows strain rates ~ 4 times slower than the Fe-rich garnet. The gray dashed line indicates the stress- and strain-rate curve of the olivine at $P = 2$ GPa.

experiments are plotted in Fig. 8 as functions of strain rate and stress; the slope gives a stress exponent $n \sim 3.4 \pm 0.7$ for garnet and $n \sim 3.7 \pm 0.8$ for olivine. Thus, our mechanical data suggests the deformation occurs by dislocation creep. The deformation microstructures, such as the dynamic recrystallization and the development of lattice-preferred orientation, also support the argument that dislocation creep is the dominant deformation mechanism for both olivine and garnet (Fig. 4). Therefore, the strength contrast in our experiments corresponds to that of the dislocation regime.

The experimental results at dry conditions show greater strain in the Fe-rich garnet than in the olivine (Fig. 7a). This indicates that a Fe-rich garnet is weaker than olivine at the given deformation conditions. The Fe-rich garnets deformed at $P = 2$ GPa show slightly higher stresses than those deformed at $P = 1$ GPa. The pressure effect seems weak under our limited experimental conditions although the estimate of the activation volume is subject to a large uncertainty due to the narrow pressure range investigated here. The Mg-rich garnets were unstable at $P = 1$ GPa, and therefore we deformed them at only $P = 2$ GPa and compared the results with the Fe-rich garnets at a same $P-T$ condition. The Mg-rich garnets show significantly smaller strain than the olivine sample (Fig. 7b), contrary to the results shown in the Fe-rich garnet. This corresponds to strain rate ~ 4 times slower in the Mg-rich garnet than the Fe-rich garnet, suggesting that the major element chemical composition influences the creep strength of the garnet. The experimental results are compared to a homologous temperature scaling law, in which the compositional effect on creep rate is inferred from the change in the melting temperature (Karato et al., 1995). The homologous temperature normalization predicts a strain rate for the Mg-rich factor is ~ 3.4 times slower than for the Fe-rich garnet, which agrees with our experimental results.

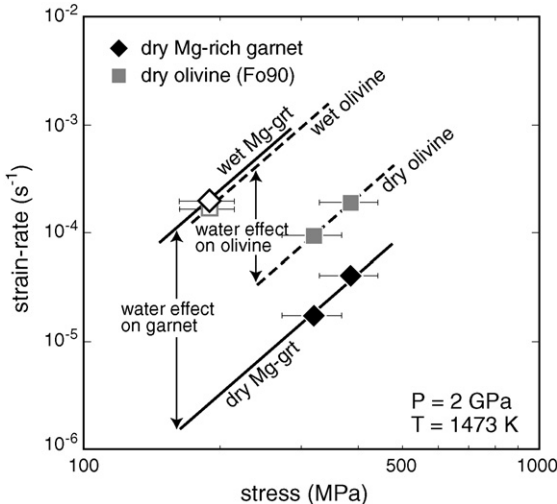


Fig. 9. Stress- and strain-rate relation of the Mg-rich garnet and olivine (Fo90) under dry ($f_{\text{H}_2\text{O}} \sim 7.2 \times 10^2 \text{ MPa}$) and wet ($f_{\text{H}_2\text{O}} \sim 4.5 \times 10^3 \text{ MPa}$) conditions. The influence of water is different between garnet and olivine; the strain rate increases by two orders of magnitude for the garnet but by an order of magnitude for the olivine under water-rich conditions.

Water also has a large effect on the creep strength of garnet. In a water-rich environment, the strains in the Mg-rich garnet and olivine are nearly identical (Fig. 7c), although in a dry environment the Mg-garnet shows significantly smaller strain than the olivine (Fig. 7b). The presence of water enhances the strain rates of both olivine and garnet, but the creep rate of garnet is more sensitive to the water content than olivine (Fig. 9). The effect of water on creep rate is usually analyzed by the power of water fugacity as follows,

$$\dot{\varepsilon} \propto f_{\text{H}_2\text{O}}^r \quad (2)$$

where $f_{\text{H}_2\text{O}}$ is the water fugacity, and r is the water fugacity exponent (Mei and Kohlstedt, 2000b; Karato and Jung, 2003). We calculated the water fugacity from the water concentration in olivine, and by comparison to the results of the water solubility experiments of Kohlstedt et al. (1996) and Zhao et al. (2004). The relationship between the normalized strain rate and the water fugacity is shown in Fig. 10. The olivine shows a water fugacity exponent of $\sim 1.2 (\pm 0.2)$, which is in good agreement with the previous studies for wet deformation experiments of olivine in the dislocation creep regime (Mei and Kohlstedt, 2000b; Karato and Jung, 2003). On the other hand, the garnet has a larger water fugacity exponent $r \sim 2.4 (\pm 0.3)$. Due to the strong influence of water on the creep strength of garnet, garnet becomes weaker than olivine at a higher water fugacity (water-rich environments).

The water fugacity exponent is related to the microscopic mechanisms of plastic deformation. At high-temperatures, the plastic deformation of a solid may be controlled by the climb motion of a dislocation. In such a case, the rate of deformation is proportional to the relevant diffusion coefficient and the density of jogs (Poirier, 1985). A range of models that are consistent with the experimental observation of $r \sim 2.4$ are shown in Table 3. The experimental results on the water fugacity exponent suggest that a concentration of $(4\text{H})_{\text{Si}}^X$ defect in garnet is likely to control the rate of deformation under hydrous condi-

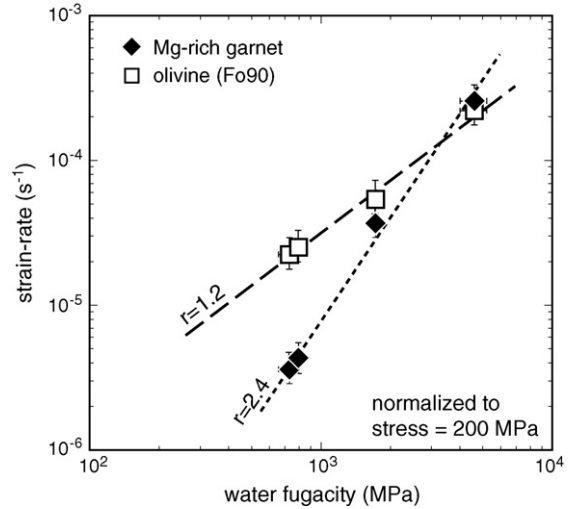


Fig. 10. Normalized strain rate as a function of water fugacity. The water fugacity exponent (r) is ~ 1.2 for olivine and ~ 2.4 for garnet. Due to the different water fugacity exponent, garnet is stronger than olivine at water-poor conditions but will be weaker than olivine at water-rich conditions.

tions, whereas the positively charged interstitial silicon $\text{Si}_i^{+\bullet\bullet\bullet\bullet}$ is the rate-controlling defect in olivine (Mei and Kohlstedt, 2000b; Karato and Jung, 2003). Alternatively, the creep rate may be controlled by dislocation glide, since garnet has a large unit cell and consequently a high Peierls stress (Karato et al., 1995). In this model, the creep rate is proportional to the mobility and the density of kinks. Heggie and Jones (1986) showed that in quartz the

Table 3
Water fugacity exponent in garnet depending on various type of point defect and jog type

Rate-limiting species	Point defect	Jog type		
		Positive	Neutral	Negative
Charge neutrality: $[\text{Fe}_M^\bullet] = [\text{HM}']$				
Si	$\text{V}_{\text{Si}}^{''''}$	-3/4	-1	-5/4
	$\text{Si}_i^{+\bullet\bullet\bullet\bullet}$	5/4	1	3/4
	$(3\text{H})_{\text{Si}}'$	3/2	5/4	1
	$(4\text{H})_{\text{Si}}^X$	9/4	2	7/4
O	V_o^{++}	3/4	1/2	1/4
	$\text{O}_i^{''}$	-1/4	-1/2	-3/4
Charge neutrality: $[\text{Fe}_M^\bullet] = [(3\text{H})_{\text{Si}}']$				
Si	$\text{V}_{\text{Si}}^{''''}$	-9/4	-3	-15/4
	$\text{Si}_i^{+\bullet\bullet\bullet\bullet}$	15/4	3	9/4
	$(3\text{H})_{\text{Si}}'$	3/2	3/4	0
	$(4\text{H})_{\text{Si}}^X$	11/4	2	5/4
O	V_o^{++}	9/4	3/2	3/4
	$\text{O}_i^{''}$	-3/4	-3/2	-9/4
Charge neutrality: $[\text{Si}_M^\bullet] = [\text{Mg}_M']$				
Si	$\text{V}_{\text{Si}}^{''''}$	0	0	0
	$\text{Si}_i^{+\bullet\bullet\bullet\bullet}$	0	0	0
	$(3\text{H})_{\text{Si}}'$	3/2	3/2	3/2
	$(4\text{H})_{\text{Si}}^X$	2	2	2
O	V_o^{++}	0	0	0
	$\text{O}_i^{''}$	0	0	0

The Kröger–Vink notation of point defect is used.

hydrated kinks have much higher mobility than the anhydrous kinks. If this model is used for garnet, our experimental observations suggest that a hydrated kink in garnet is formed when the Si-site is replaced with four protons.

4. Discussion

4.1. Comparison to other experiments

The results of our experiments on the creep strength of garnet are compared to the previous experiments in the dislocation creep regime (Fig. 11). Karato et al. (1995) systematically analyzed the creep strength of silicate garnet as well as analogue materials with garnet structure (Karato et al., 1995). They found that the rheological behaviors of garnet follow the homologous temperature scaling law, in which the creep strength is characterized by the shear modulus μ and the melting temperature T_m ,

$$\dot{\varepsilon} = B \left(\frac{\sigma}{\mu} \right)^n \exp \left(-g \frac{T_m}{T} \right) \quad (3)$$

where B and g are constants (Karato et al., 1995). This scaling law expresses the effects of pressure, temperature and the compositional variations through the changes of melting temperature and shear modulus. The data on the Alm-Prp garnet at low-pressure (Karato et al., 1995) is normalized to $T_m/T=1.14$ and the stress is normalized by the shear modulus in Fig. 11. The results show that our experimental data on the anhydrous Fe-rich garnet are in good agreement with their experiments on the Alm-Prp garnet. In addition, the difference in the creep strength between the Fe-rich and the Mg-rich garnets in our experiments is well explained by the homologous temperature

scaling law through the difference in their melting temperature. In contrast, the results from high-pressure deformation experiments of pyrope using a D-DIA ($P=4.3\text{--}6.8\text{ GPa}$; Li et al., 2006) show a significantly higher creep rate than in our experiments (Fig. 11). This discrepancy may be due to the relatively high water content in their experiments, as they reported water contents of $\sim 35\text{ ppm H}_2\text{O}$ by weight (corresponds to $\sim 600\text{ ppm H/Si}$) in their deformed samples. The creep data for eclogite reported by Jin et al. (2001) seems similar to our experiments (Fig. 11), however the eclogite is mainly composed of omphacite and garnet and it can be weaker than the monophase of garnet. Trace amounts of water were initially included in the eclogite samples ($100\text{--}200\text{ ppm H}_2\text{O}$ by weight; Jin et al., 2001) and consequently the specimens may have been subject to partial melting at their experimental conditions, $P=3\text{ GPa}$ and $T=1450\text{--}1600\text{ K}$. Such conditions are well above the melting curve of eclogite under hydrous conditions (Poli and Schmidt, 1995). Water is preferentially partitioned into a melt phase and hence the water-loss hardening might occur during these experiments. Small amounts of a melt phase will reduce the creep strength (Hirth and Kohlstedt, 1995), but water has a strong influence on the creep strength of garnet and the water loss due to a partial melting could result in the mechanical hardening of the samples.

4.2. Deformation of garnet in natural samples

Garnet is considered to be one of the strongest silicate minerals among crustal and mantle rocks, and the isotropic optical properties of garnet have hindered the study of its deformation features. However, recent detailed microstructural analysis shows evidence of the plastic deformation of garnet. EBSD and the orientation contrast imaging studies showed subgrain microstructures in naturally deformed garnets from high-temperature crustal metamorphic rocks and in deep mantle peridotites (Prior et al., 2000; Kleinschrodt and MaGrew, 2000; Michibayashi et al., 2004; Terry and Heidelbach, 2004; Katayama et al., 2005). This indicates deformation that involves dislocation climb and recovery. The crystal preferred orientation of the naturally deformed garnet is relatively weak due to its cubic symmetry, but some samples show a degree of preferred orientation with a dominant slip system of $1/2\langle 1\ 1\ 1 \rangle \{ 1\ 1\ 0 \}$ (Kleinschrodt and Duyster, 2002; Mainprice et al., 2004). The dislocation microstructures of the natural garnets, observed by a transmission electron-microscope (TEM), show evidence of a dominant Burgers vector of $\langle 1\ 0\ 0 \rangle$ at low stress (in terms of low dislocation density) and $1/2\langle 1\ 1\ 1 \rangle$ at high stress (Ando et al., 1993). Ji and Martignole (1994) suggested that flattened garnets in high-temperature quartz-felspathic mylonites were evidence of plastic deformation accommodated by the dislocation recovery. For the mantle peridotites, the garnets in cratonic xenoliths are nearly isotropic and are not highly deformed, whereas the associated olivine matrix has been extensively deformed with the dynamic recrystallization and the significant lattice-preferred orientation (e.g., Mercier, 1985). In contrary to this, some garnets in the Alpine-type peridotites are highly elongated and show the internal subgrain-boundaries (Katayama et al., 2005).

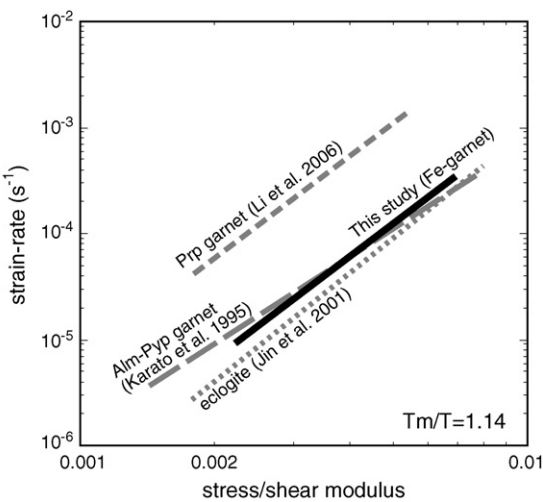


Fig. 11. Comparison of the normalized creep strength of garnet with the previous experiments in the dislocation creep regime. The dry Fe-rich garnet (this study) has similar creep strength of Alm-Prp garnet (Karato et al., 1995), but the results from pyrope garnet (Li et al., 2006) are significantly weaker than our data (see text for more detail). The creep test of eclogite by Jin et al. (2001) shows similar strength to our Fe-rich garnet although the eclogite is mainly composed of garnet and omphacite.

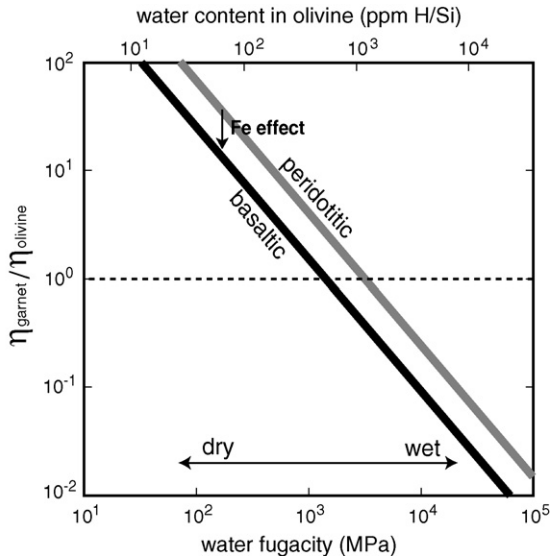


Fig. 12. Viscosity contrast between olivine and garnet as a function of water fugacity (we assumed a constant stress of 10 MPa. However, either stress is constant or strain rate is constant does not affect the results so much because the stress exponent is similar between the two minerals). The chemical composition of garnet is normalized to the basaltic composition by the effect of the Fe component (black thick line). The viscosity contrast depends strongly on the water fugacity, i.e., garnet is weaker than olivine under water-rich conditions, whereas olivine will be weaker than garnet under dry conditions. The gray region is the condition where garnet is weaker than olivine. The critical water fugacity is $f_{\text{H}_2\text{O}} \sim 10^3$ MPa, which corresponds to $\text{COH} \sim 300$ ppm H/Si in olivine.

Our experimental results showed that water has a strong influence on the plastic strength of garnet, and that the difference in the creep strength of the naturally deformed garnets can be explained by the influence of water. Alpine-type peridotites occur in the plate-convergent regions, where high water contents are expected, and consequently garnet in such regions could be weak and easily deformed. In contrast, the garnets in cratonic xenoliths are significantly stronger than olivine due to the highly depleted environments (water poor) in the continental lithosphere.

4.3. Geophysical implications

The application of our results to the deformation in the shallow upper mantle is straightforward. We have calculated the relative viscosity of garnet and olivine at $P=2$ GPa and $T=1473$ K as a function of water content (Fig. 12). If water fugacity is higher than $\sim 10^3$ MPa (corresponds to $\text{COH} \sim 300$ ppm H/Si in olivine), the garnet-rich layer is expected to be weaker than the surrounding mantle. In contrast, below the critical water fugacity ($f_{\text{H}_2\text{O}} \sim 10^3$ MPa), the garnet layer becomes stronger than the surrounding mantle. Here we define the relative viscosity as $\eta_{\text{olivine}}/\eta_{\text{garnet}} = \dot{\varepsilon}_{\text{garnet}}/\dot{\varepsilon}_{\text{olivine}}$ where $\eta = \sigma/\dot{\varepsilon}$ is the effective viscosity. Water content in the upper mantle is thought to be regionally different, i.e., asthenospheric mantle contains ~ 1000 ppm H/Si whereas water content in the lithospheric mantle should be lower by a couple orders of magnitude (Hirth and Kohlstedt, 1996; Karato and Jung, 1998). The garnet-rich components will therefore be well mixed in

the asthenosphere (water-rich region) by the mantle convection, whereas they remain unmixed in the depleted regions (i.e., lithosphere).

The application of the current data to the rheological behavior of garnet-rich regions in the deep upper mantle is not straightforward because the influence of pressure on the rheological properties of these two minerals is not well known. However, detailed experimental work on garnet has shown that garnets follow the homologous temperature scaling law (Karato et al., 1995). Consequently, we may use the homologous temperature scaling to estimate the influence of pressure on the relative strength of garnet and olivine. Based on the pressure derivatives of the melting temperature of garnet and olivine (Irfune and Ohtani, 1986), the viscosity contrast $\eta_{\text{olivine}}/\eta_{\text{garnet}}$ is expected to be one order of magnitude smaller at $P=10$ GPa than at $P=2$ GPa (our experimental condition). Thus, the pressure has a larger effect on the rheological contrast to make garnet stronger relative to olivine, but water always has a large effect, as water contents can be different by a couple orders of magnitude. We therefore suggest that the conclusion reached above will also apply under the deep mantle conditions, although the range of conditions where garnet is stronger than olivine is somewhat expanded under the deep mantle conditions.

Oceanic crust that has been deeply subducted is mostly composed of garnet, and this layer becomes less dense than the surrounding mantle at the base of upper mantle. Because of this density crossover between the crust and mantle, it has been proposed that the crustal component might be separated from the descending slab and gravitationally trapped at the mantle transition zone (e.g., Ringwood and Irfune, 1988). The process of separation of the oceanic crust from the descending slabs is largely controlled by the viscosity contrast between these two components. The separation is possible when a garnet-rich paleo-oceanic crust has a somewhat higher viscosity than the layer below (van Keken et al., 1996; Karato, 1997), whereas the separation does not occur when the viscosity between the two layers is similar (Richards and Davies, 1989). Our experimental results cannot be directly applied to such deep mantle conditions, however water has a large influence on the rheological properties of a garnet-rich layer and the separation condition will be sensitive to water content. If water has a stronger influence on the creep strength of garnet than the surrounding materials as shown in this study, the separation of the subducted crust could occur when the subducted crust is relatively low water content (and therefore high viscosity), whereas the separation will not occur when it has a high water content.

Acknowledgments

We thank Y. Nishihara and P. Skemer for discussion, and Z. Jiang, K. Michibayashi and T. Kuwatani for technical assistance. We also appreciate T. Mitchell for English correction in the manuscript. Comments by G. Hirth, D. Rubie and anonymous reviewers were helpful to improve the manuscript. This study was supported by US National Science Foundation grants (to S. Karato) and by a research fellowship from Japan Society for the Promotion of Science (to I. Katayama).

References

- Ackermann, L., Cemic, L., Langer, K., 1983. Hydrogarnet substitution in pyrope: a possible location for water in the mantle. *Earth Planet. Sci. Lett.* 62, 208–214.
- Ando, J., Fujino, K., Takeshita, T., 1993. Dislocation microstructures in naturally deformed silicate garnets. *Phys. Earth Planet. Int.* 80, 105–116.
- Bell, D.R., Ihinger, P.D., Rossman, G.R., 1995. Quantitative analysis of trace OH in garnet and pyroxenes. *Am. Mineral.* 80, 465–474.
- Green, H.W., Borch, R.S., 1989. A new molten salt cell for precision stress measurement at high pressure. *Eur. J. Mineral.* 1, 213–219.
- Heggie, M., Jones, R., 1986. Models of hydrolytic weakening in quartz. *Phil. Mag. Ser. A* 53, 65–70.
- Hirth, G., Kohlstedt, D.L., 1995. Experimental constraints on the dynamics of the partially molten upper mantle. 2. Deformation in the dislocation creep regime. *J. Geophys. Res.* 100, 15441–15449.
- Hirth, G., Kohlstedt, D.L., 1996. Water in the oceanic upper mantle: implications for rheology melt extraction and the evolution of the lithosphere. *Earth Planet. Sci. Lett.* 144, 93–108.
- Irifune, T., Ohtani, E., 1986. Melting of pyrope $Mg_3Al_2Si_3O_{12}$ up to 10 GPa: possibility of a pressure-induced structural change in pyrope melt. *J. Geophys. Res.* 91, 9357–9366.
- Irifune, T., Ringwood, A.E., 1987. Phase transformations in primitive MORB and pyrolite compositions to 25 GPa and some geophysical implications. In: Manghnani, M.H., Syono, Y. (Eds.), High-Pressure Research in Mineral Physics. American Geophysical Union, Washington, DC, pp. 231–242.
- Ji, S., Martignole, J., 1994. Ductility of garnet as an indicator of extremely high temperature deformation. *J. Struct. Geol.* 16, 985–996.
- Jin, Z.M., Zhang, J., Green, H.W., Jin, S., 2001. Eclogite rheology: implication for subducted lithosphere. *Geology* 29, 667–670.
- Karato, S., 1987. Scanning electron microscope observation of dislocations in olivine. *Phys. Chem. Miner.* 14, 245–248.
- Karato, S., 1997. On the separation of crustal component from subducted oceanic lithosphere near the 660 km discontinuity. *Phys. Earth Planet. Int.* 99, 103–111.
- Karato, S., 2008. Deformation of Earth Materials: An Introduction to the Rheology of Solid Earth. Cambridge Univ. Press, New York, 562 p.
- Karato, S., Jung, H., 1998. Water, partial melting and the origin of the seismic low velocity and high attenuation zone in the upper mantle. *Earth Planet. Sci. Lett.* 157, 193–207.
- Karato, S., Jung, H., 2003. Effects of pressure on high-temperature dislocation creep in olivine. *Phil. Mag. A* 83, 401–414.
- Karato, S., Wang, Z., Liu, B., Fujino, K., 1995. Plastic deformation of garnets: systematics and implications for the rheology of the mantle transition zone. *Earth Planet. Sci. Lett.* 130, 13–30.
- Karato, S., Paterson, M.S., FitzGerald, J.D., 1986. Rheology of synthetic olivine aggregates: influence of grain size and water. *J. Geophys. Res.* 91, 8151–8176.
- Katayama, I., Karato, S., Brandon, M., 2005. Evidence of high water content in the deep upper mantle inferred from deformation microstructures. *Geology* 33, 613–616.
- Kleinschrodt, R., MaGrew, A.J., 2000. Garnet plasticity in the lower continental crust: implications for deformation mechanisms based on microstructures and SEM electron channeling pattern analysis. *J. Struct. Geol.* 22, 795–809.
- Kleinschrodt, R., Duyster, J.P., 2002. HT-deformation of garnet: an EBSD study on granulites from Sri Lanka, India and the Ivrea Zone. *J. Struct. Geol.* 24, 1829–1844.
- Kohlstedt, D.L., Keppler, H., Rubie, D.C., 1996. Solubility of water in the α , β and γ phases of $(Mg, Fe)_2SiO_4$. *Contrib. Mineral. Petrol.* 123, 345–357.
- Li, L., Long, H., Raterron, P., Weidner, D., 2006. Plastic flow of pyrope at mantle pressure and temperature. *Am. Mineral.* 91, 517–525.
- Mainprice, D., Bascou, J., Cordier, P., Tommasi, A., 2004. Crystal preferred orientation of garnet: comparison between numerical simulations and electron back-scattered diffraction (EBSD) measurements in naturally deformed eclogites. *J. Struct. Geol.* 24, 2089–2102.
- Manga, M., 1996. Mixing of heterogeneities in the mantle: effect of viscosity differences. *Geophys. Res. Lett.* 23, 403–406.
- Mei, S., Kohlstedt, D.L., 2000a. Influence of water on plastic deformation of olivine aggregates. 1. Diffusion creep regime. *J. Geophys. Res.* 105, 21457–21469.
- Mei, S., Kohlstedt, D.L., 2000b. Influence of water on plastic deformation of olivine aggregates. 2. Dislocation creep regime. *J. Geophys. Res.* 105, 21471–21481.
- Mercier, J.C., 1985. Olivine and pyroxenes. In: Wenk, H.R. (Ed.), An Introduction to Modern Texture Analysis. Academic Press, San Diego, pp. 407–430.
- Michibayashi, K., Okamoto, A., Masuzawa, T., Kawakami, T., Ikeda, T., Yasuda, H., 2004. Orientation contrast images of garnet from granulite quartzite, Lutzow-Holm Complex, East Antarctica. *J. Geol. Soc. Jpn.* 110, 5–6.
- Paterson, M.S., 1982. The determination of hydroxyl by infrared absorption in quartz, silicate glasses and similar materials. *Bull. Mineral.* 105, 20–29.
- Poirier, J.P., 1985. Creep of Crystals. Cambridge Univ. Press, New York, 260 p.
- Poli, S., Schmidt, M.W., 1995. H_2O transport and release in subduction zones: experimental constraints on basaltic and andesitic systems. *J. Geophys. Res.* 100, 22299–22314.
- Prior, D.J., Wheeler, J., Brenker, F.E., Harte, B., Matthews, M., 2000. Crystal plasticity of natural garnet: new microstructural evidence. *Geology* 28, 1003–1006.
- Richards, M.A., Davies, G.F., 1989. On the separation of relatively buoyant components from subducted lithosphere. *Geophys. Res. Lett.* 16, 831–834.
- Ringwood, A.E., Irifune, T., 1988. Nature of the 650-km seismic discontinuity—implications for mantle dynamics and differentiation. *Nature* 331, 131–136.
- Terry, M.P., Heidelbach, F., 2004. Superplasticity in garnet from eclogite facies shear zones in the Haram Gabbro, Haramsoya, Norway. *Geology* 32, 281–284.
- van Keken, P.E., Karato, S., Yuen, D.A., 1996. Rheological control of oceanic crust separation in the transition zone. *Geophys. Res. Lett.* 23, 1821–1824.
- Zhang, S., Karato, S., FitzGerald, J.F., Faul, U.H., Zhou, Y., 2000. Simple shear deformation of olivine aggregates. *Tectonophysics* 316, 133–152.
- Zhao, Y.H., Ginsberg, S.B., Kohlstedt, D.L., 2004. Solubility of hydrogen in olivine: dependence on temperature and iron content. *Contrib. Mineral. Petrol.* 147, 155–161.